DOI: 10.13009/EUCASS2019-586

Experimental validation of an aeroelastic reduced order model dedicated to high aspect ratio flexible composite wing

Bertrand Kirsch[⋆], *Olivier Montagnier*[⋆], *Emmanuel Bénard*[⋆†], *Thierry M. Faure*[⋆]
[⋆]*Centre de Recherche de l'École de l'Air*
École de l'Air, 13661 Salon Air, France
bertrand.kirsch@ecole-air.fr · olivier.montagnier@ecole-air.fr · thierry.faure@ecole-air.fr
[†]*Institut Supérieur de l'Aéronautique et de l'Espace - Supaéro*
10 avenue Édouard-Belin, BP 54032 - 31055 Toulouse CEDEX 4
emmanuel.benard@isae.fr

Abstract

The enhancement of high altitude drone endurance compels to design very flexible high-aspect-ratio composite airframe vulnerable to destructive fluid/structure interaction like flutter or torsional divergence. Extensive research has been conducted to increase critical speed without being at the expense of weight balance. One of the promising solutions is the aeroelastic tailoring which consists in a specific configuration of laminated composite layup. The present work uses an aeroelastic reduced order model, namely GEBTAero, suitable for the non linear anisotropic behavior of this kind of composite wing, able to quickly compute aeroelastic critical speeds. Particular focus is put on a wind tunnel test campaign conducted on a set of three-ply composite flexible plates, in order to assess the accuracy of GEBTAero.

1. Introduction

Recent progress made in the field of solar cells, energy storage and composite materials pave the way to a new concept of aircraft, namely High Altitude Pseudo Satellite (HAPS). Among them, a particular type of solar or/and hydrogen powered High Altitude Long Endurance (HALE) Unmanned Aerial Vehicles (UAV) aims to meet a virtually infinite endurance. To achieve this far-reaching goal, aerodynamic and structural performances are stretched to their limits because of the low on-board power. This results, on the aerodynamic side, in high-aspect ratio wing optimising the lift-to-drag ratio and, on the structural side, in lightweight very flexible composite airframe. The main drawback of this particular design is its vulnerability to destructive fluid/structure interactions like torsional divergence and flutter which are difficult to predict because of the tight coupling between aerodynamics, structure and flight mechanics. Classical solutions designed to further aeroelastic critical speed mostly rely on the stiffening of the airframe or the adjustment of mass distribution. Both options are detrimental to mass balance, which is a key feature of HAPS. In that context, alternative solutions should be explored, among these are active flutter suppression and aeroelastic tailoring. For the first one, the reader is referred to a thorough review proposed by Livne.[15] The present work focuses on the second one, namely aeroelastic tailoring, which is a technology born in the 1970s with the forward-swept wing experimental plane X-29. It consists in using laminate layup without mirror symmetry and/or unbalanced layup. The emerging structural coupling induced on the aerodynamic side a coupling between the bending, due to lift forces, and the twisting of the wing which determines the local Angle of Attack (AoA) and consequently an impact on aeroelastic behavior.

The computational cost of high fidelity aeroelastic simulation on Very Flexible Aircraft (VFA) is still prohibitive, prompting the need for suitable reduced order model. Many reduced order model tools have been developed during the last decades. We could mention computation code NANSI (Nonlinear-Aerodynamics/ Nonlinear-Structure Interaction)[23] which combines an Unsteady Vortex Lattice Method (UVLM) and a nonlinear beam theory. The UVLM is particularly useful in case of low-aspect-ratio wing or delta wing because the method is able to predict 3D effects. Another solution is proposed by Murua in SHARP program (Simulation of High Aspect Ratio Planes)[16] using UVLM with a displacement based geometrically exact beam theory. Because of the high aspect ratio of VFA wings, a lot of models rely on the coupling between a beam theory on the structural side and an unsteady aerodynamic strip theory on the aerodynamic side. This is the case of ASWING developed by Drela[5] combining a nonlinear isotropic beam formulation with an unsteady lifting line theory. UM/NAST (University of Michigan/ Nonlinear Aeroelastic Simulation Toolbox), developed by Shearer and Cesnik[20] uses a strain-based geometrically nonlinear beam formulation linked with a finite

DOI: 10.13009/EUCASS2019-586

state two-dimensional incompressible flow aerodynamic theory proposed by Peters et al.[18] A similar formulation is used by Ribeiro in the Matlab toolbox Aeroflex.[19] One last example is the Matlab toolbox NATASHA (Nonlinear Aeroelastic Trim and Stability of HALE Aircraft)[3] which relies on an intrinsic beam formulation coupled with Peters' theory. In the present work, GEBTAero,[10, 12] developed by the author, extends the structural solver GEBT developed by Yu and Blair[24] and Wang et al.[22] with a tight coupling with Peters theory in an open source implementation dedicated to high aspect ratio composite wing optimisation using aeroelastic tailoring.

Every computation code need to be evaluated against test cases. The most famous aeroelastic test case is probably the Goland wing,[6] with the advantage of being widely used is the community but which is not adapted to VFA (flutter speed is high for incompressible hypothesis and the wing is not flexible). More recently, the Patil wing[17] proposes a more suitable test case to asses the impact of geometrical non linearities on aeroelastic behaviour, but still with an isotropic wing. GEBTAero has been tested against this two test cases with a good agreement.[13] On the experimental side, there is only little data available in the literature concerning flexible wings. We could mention the wind tunnel test conducted by Tang and Dowell[21] on a flexible wing made of a steel flat plate with a balsa wing skin. Although this experiment give interesting results, notably in terms of Limit Cycle Oscillation (LCO) studies, the aeroelastic tailoring effect is not taken into account on this isotropic wing.

This paper presents a wind tunnel test campaign conducted on three-ply flexible laminates. First, the aeroelastic reduced order model used in GEBTAero is detailled. Then, after a short presentation of the experimental setup, experimental results for laminates with different layups are provided and the agreement with the numerical results is discussed.

2. Aeroelastic reduced order model

The main objective of GEBTAero is to define a fast implementation of a proper reduced order aeroelastic model well fitted for the computationally intensive task of aeroelastic tailoring optimisation. It relies on the use of optimised open source programs and libraries (sparse direct linear solver MUMPS,[1] sparse eigenvalues solver ARPACK[14]).

The high-aspect-ratio wing assumption gives us the opportunity to neglect three-dimensional effects and thus to use a strip theory which can be easily linked to a beam formulation. A tight coupling is chosen, done by integrating aerodynamic loads directly into the weak formulation of the beam theory. It permits the determination of the aeroelastic modes of the wing about a geometrically non linear steady state, namely frequencies, modal shapes and damping factors. The latter is a key parameter for our study, because it defines the limit between stable and unstable speed.

On the structural side, to ensure a proper modelling of the laminate anisotropy and geometrical non linearity, the choice fell on an open source tool named GEBT (Geometrically Exact Beam Theory) developed by Yu and Blair[24] and Wang et al.[22] designed for composite slender structures under large deflections and rotations, assuming the strains to be small. This tool coded in Fortran 90/95 implements a mixed variational formulation based on exact intrinsic equations for dynamics of moving beams developed by Hodges.[7] The main strength of this method, compared to classical displacement based formulation, is to avoid the dependency from a coordinate system (intrinsic nature) for the position and rotation parameters. Kinematical and constitutive relations are then added to the weak formulation with Lagrange multipliers (mixed nature). The resulting formulation allows a finite element implementation with very simple shape functions (constant or linear).

Because of the large displacement and rotation of the wing, three different frame are required (figure 1a):

- a unique global body attached frame a $(\vec{x}_a, \vec{y}_a, \vec{z}_a)$ moving with a given linear and angular velocity $\vec{v}_a$ and $\vec{\omega}_a$ in an inertial frame and consistent with flight mechanics conventions ($\vec{x}_a$ pointing upwards, $\vec{y}_a$ pointing the right wing and $\vec{z}_a$ pointing downwards);

- at least one undeformed beam frame b $(\vec{x}_b, \vec{y}_b, \vec{z}_b)$ fixed in frame a: $\vec{x}_b$ is tangent to the reference line of the undeformed beam. In our case, a frame b is defined for each section of the wing with a different dihedral or/and wing-sweep;

- a deformed beam frame B $(\vec{x}_B, \vec{y}_B, \vec{z}_B)$ for each beam element: $\vec{x}_B$ is tangent to the deformed beam reference line and points to the right, $\vec{y}_B$ has a chordwise direction and points the upstream flow and $\vec{z}_B$ completes the triad.

The cross section parameters of the anisotropic beam are determined using an homogenisation tool following a method developed by Cartraud and Messager.[2] It consists in a three-dimensional finite element calculation realized with the open source solver CalculiX[4] on a Representative Volume Element (RVE) of the beam using periodic boundary conditions along beam axis direction.[10] The RVE is a 3D mesh written in Abaqus input format. Different cases are considered:

DOI: 10.13009/EUCASS2019-586

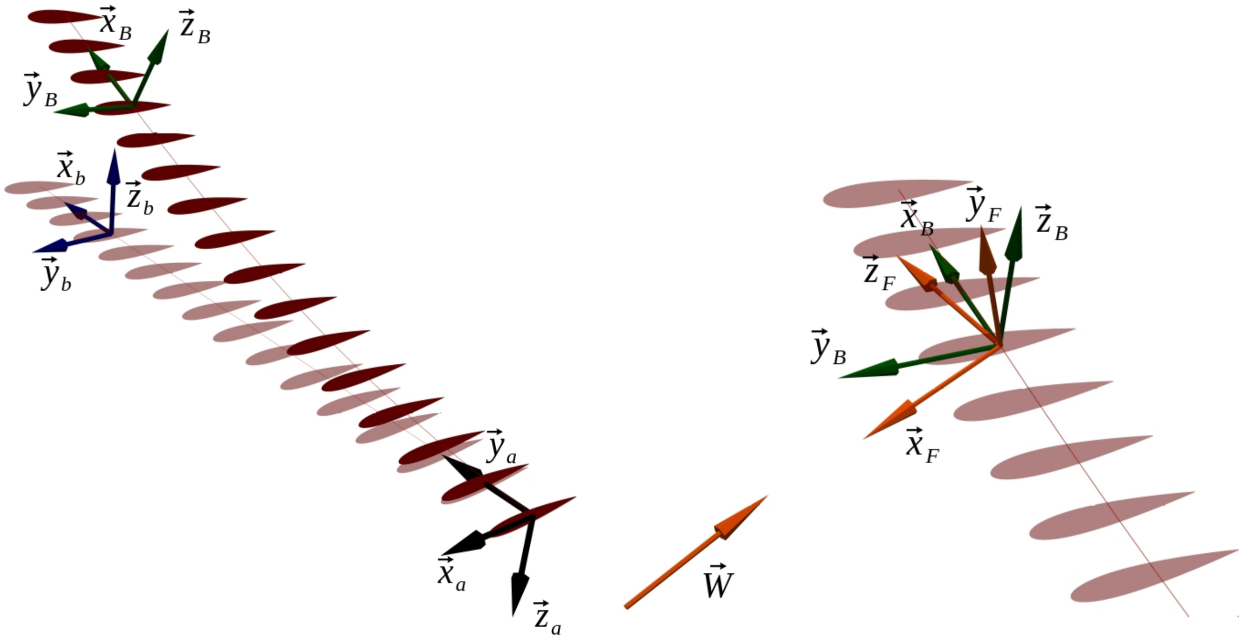

(a) (b)

Figure 1: Frames definition: a) structural frames, b) aerodynamic frame.

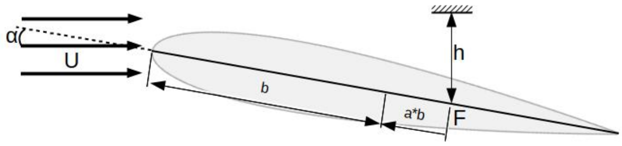

Figure 2: Airfoil parameters.

- simple shape constant cross section (plate or box): the mesh is automatically generated using the pre/postprocessor CalculiX GraphiX;
- constant cross section: a 2D mesh is extruded with a unique element spanwise;
- periodic cross section: a wing section representing a beam period is meshed (between two ribs for instance).

At the end, the homogenisation step provides, for each section with different shape, an inertia matrix $\vec{\vec{I}}$ and a flexibility matrix $\vec{\vec{S}}$.

On the aerodynamic side , the unsteady two-dimensional finite state approximation model developed by Peters et al.[18] is used. This formulation is implemented in our toolbox with the following aerodynamic loads:

$$L = \pi\rho b^2 \left(\ddot{h} + U\dot{\alpha} - ba\ddot{\alpha}\right) + 2\pi\rho U b \left[\dot{h} + U\alpha + b\left(\frac{1}{2} - a\right)\dot{\alpha} - \lambda_0\right] \tag{1}$$

$$M = b\left(\frac{1}{2} + a\right)L - \pi\rho b^3 \left[\frac{1}{2}\ddot{h} + u\dot{\alpha} + b\left(\frac{1}{8} - \frac{a}{2}\right)\ddot{\alpha}\right] \tag{2}$$

with L the linear lift, M the linear moment around a reference point F, ρ the air density and U the flow velocity. The semi-chord b, the height h, AoA α and the distance a between the point F and the semi-chord are detailed in Fig. 2.

The induced-flow velocity λ_0 is approximated using N_S induced-flow states $\lambda_1, \lambda_2, \ldots, \lambda_{N_S}$ by:

$$\lambda_0 \approx \frac{1}{2}\sum_{n=1}^{N_S} b_n \lambda_n$$

DOI: 10.13009/EUCASS2019-586

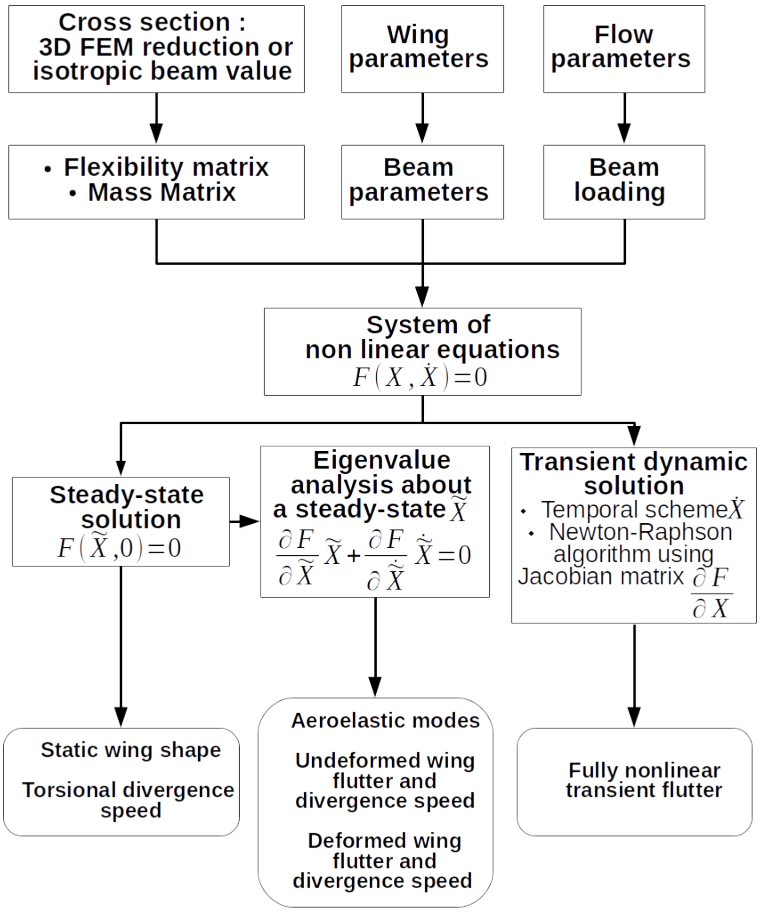

Figure 3: GEBTAero computation features.

where the b_n are found in[8] by the least-square method. The λ_n are determined using a set of N_S first-order ODEs as detailled in.[8] The aerodynamic model adds N_S equations for each beam element, the coupled aeroelastic system contains $(18 + N_S)\,N+12$ equations and the same number of unknowns with N the number of beam elements, providing that structural unknowns are completed with $N \times N_S$ induced-flow states λ_{n_i}.

The tight coupling between structural and aerodynamic models is done using a forth frame F $(\vec{x}_F, \vec{y}_F, \vec{z}_F)$ defined in figure 1b. The resulting formulation permits different applications both in time domain and frequency domain. The capabilities of the resulting program called "GEBTAero"[9] are summarize in figure 3. A particular aspect of this computation code is its capability to quickly compute critical speeds, thanks notably to a modal resolution strategy based on the computation of only a few modes of interest using Arpack modal solver, and the use of sparse matrix.[12]

3. Experimental results

3.1 Experimental setup

The experimental campaign is conducted in a wind tunnel with a test section of $450 \times 450 \times 650$ mm and a speed range from 5 to 45 m/s. The flat plate is mounted using a 3D printed device linked to the side wall of the wind tunnel. The AoA is adjustable using a rotating disk mounted on an axis (figure 4). Thereafter, all the tests are done with an AoA set to zero. The mean flow speed is measured using a differential pressure sensor between the inlet and the outlet of the nozzle placed upstream of the test section. In order to evaluate the accuracy of flutter speeds computed by GEBTAero, this experiment focuses on the flutter boundary without the need of studying LCO. In this regard, flat plates could be a good choice. Indeed, provided that the relative thickness is small enough to avoid the need for a milled leading edge and trailing edge, flat plates are good candidates for test cases because of their simplicity. The elastic, inertial and geometrical parameters are easy to determine and the shape is adapted to aerodynamic model as long as the angle of attack remains small.

DOI: 10.13009/EUCASS2019-586

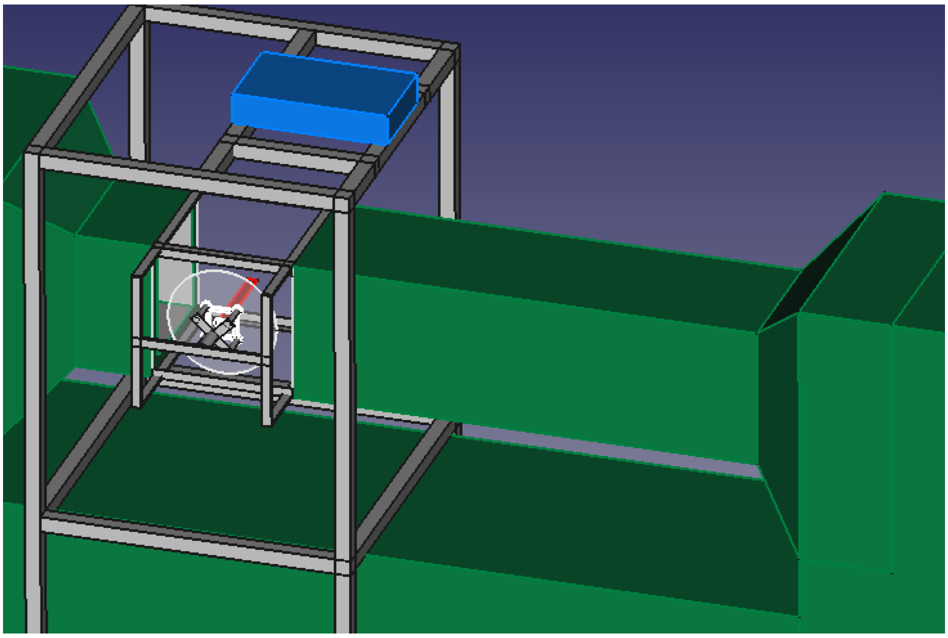

Figure 4: Overview of the experimental set-up.

Concerning the measurements, the large displacement and rotation of the plate, the flexibility and the small weight of such a plate make it difficult to choose a proper type of sensors to assess flutter speed and frequency. To tackle those constraints, two micro-accelerometers are used (B&K DeltaTron type 4517 : 0, 65 g, $8.15 \times 6.35 \times 3.8$ mm, bandwidth 1 Hz to 20 kHz). They are little intrusive and allow to retrieve speed and displacement data throw the integration of the signal.

A first campaign on flexible metallic plate (aluminium) has been conducted,[11] showing a good agreement between the experimental and numerical flutter speed, providing that the geometrical non linearities due to the effect of gravity is taken into account.

3.2 Flexible composite plates

In order to evaluate the anisotropic capability of GEBTAero, a second wind tunnel campaign is conducted on flexible laminate plates with bending/twisting coupling. The UniDirectional (UD) prepreg used is a UD150/CHS/M10R, its characteristics are presented in table 1. In the same way as for metallic plates, simple solutions are seeking to produce relevant test cases. A laminate layup is defined by the orientation of its plies $[\theta_1, \ldots, \theta_n]$. According to the Classical Laminate Theory (CLT), a laminate without mirror symmetry, i.e. without symmetrical plies to the middle plan with the same orientation, has a traction/twisting coupling. This coupling could be exploited in a wing box configuration, providing that the bending of the wing produces a traction or a compression of the upper side and lower side. Thin plates exploit another type of coupling, generated by unbalanced layup, i.e. without a balance between positive and negative orientation. For example, for a balanced layup, every 45° oriented ply is compensated by a −45° ply.

Table 1: Prepreg HexPly UD150/CHS/M10R characteristics.

	unit	value
mass per unit area	g/m^2	150
nominal cured ply thickness	mm	0.16
nominal fiber volume	%	0.52
nominal laminate density	g/cm^3	1.57
longitudinal Young's modulus E_l (fiber fraction 52%)	Mpa	125
transverse Young's modulus E_t (fiber fraction 52%)	Mpa	9.3
Coulomb's modulus G_{lt}	Mpa	7.75

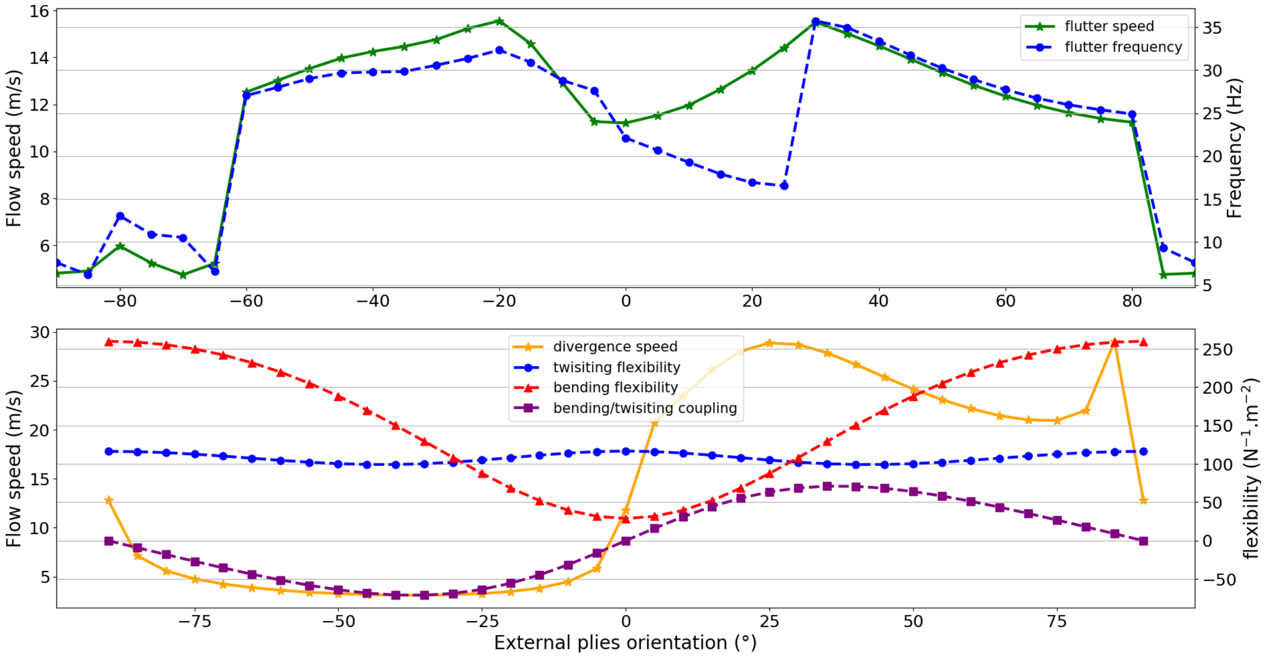

Figure 5: 420 mm half-span laminate with a central ply oriented at 0° and two external plies with various orientation: flutter speed and frequency, divergence speed and flexibility.

The simplest unbalanced layup consists in a laminate with a single orientation. Although it permits to produce a bending/twisting coupling, such a flexible plate is too fragile and may break between two fibers. The next configuration in terms of complexity is a two-ply laminate with two different fiber orientations. In that case, because mirror symmetry is not respected, the large difference between longitudinal and transverse coefficient of thermal expansion produces an undesired twisting of the plate during the cool down. Then, the simplest usable layup consists in a three-ply laminate with external plies oriented in the same direction. To obtain the proper static deflection and for sturdiness purposes, the central ply is oriented at 0°. The divergence and flutter speed, the flutter frequency and the flexibility matrix coefficients simulated by GEBTAero for different external plies orientations are plotted in figure 5. The half-span is set to 420 mm in order to alleviate wind tunnel test section side effect.

According to the simulation, five layups are produced : $[15, 0, 15]$, $[30, 0, 30]$, $[45, 0, 45]$, $[60, 0, 60]$ and $[90, 0, 90]$, allowing to simulate various aeroelastic behaviours. A sixth one is produced to evaluate another central ply orientation, namely $[30, -30, 30]$. Theoretically, it gives us five more layup by returning the plate ($[15, 0, 15]$ becomes $[-15, 0, -15]$). In fact, negative external plies orientation implies a very low divergence speed with massive stall and is therefore unusable. To illustrate the structural coupling of this laminates, static deflection of plates are shown in figure 6. Beyond the obvious discrepancy in term of bending flexibility, it shows us the structural coupling between the bending due to weight and the twisting of the cross section (except from the uncoupled $[90, 0, 90]$ laminate).

The flow speed measurement is synchronised with the acceleration measurement, allowing us to produce a spectrogram. During the test, the flow speed is slowly increased until flutter instability and then decreased. The mean flow speed is plotted in the spectrogram. In order to emphasis the complex aeroelastic behaviour encountered on flexible anisotropic plates, the results for the layups $[30, 0, 30]$ and $[30, -30, 30]$ are plotted in figures 7 and 8, compared to the aeroelastic modes plotted by GEBTAero using $N = 40$ beam elements and $N_S = 6$ induced flow states.

To illustrate how the mode plotting done by GEBTAero works, computation points are represented on the curves (figures 7c and 8c). The flow speed step is automatically adjusted to follow the different aeroelastic modes (frequency and damping) depending on the aerodynamic speed. In particular, this algorithm permits to highlight the specific interaction between the third and forth mode (classified in ascending order for frequency) characterised by a permutation of the reduced damping curves and of the frequency slopes.

Although inertial parameters are the same and flexibility matrix are close (table 2) , both layups show quite different aeroelastic behaviour. The $[30, 0, 30]$ layup shows a non linear flutter instability with harmonics and a large hysteresis in aerodynamic speed (flutter starts at 14 m/s and stops at 9 m/s). However, the $[30, -30, 30]$ layup is characterised by a wide spectrum chaotic instability but with only a small hysteresis in aerodynamic speed.

Finally, flutter speeds (figure 9) and frequencies (figure 10) are compared to the values simulated by GEBTAero for

DOI: 10.13009/EUCASS2019-586

Figure 6: Laminate static deflection, from left to right : $[90, 0, 90]$, $[60, 0, 60]$, $[45, 0, 45]$, $[30, -30, 30]$, $[30, 0, 30]$ and $[15, 0, 15]$.

Table 2: Flexibility matrix coefficients of $[30, 0, 30]$ and $[30, -30, 30]$ layups.

	unit	$[30, 0, 30]$	$[30, -30, 30]$
twisting flexibility	$N^{-1}.m^{-2}$	103.9	85.2
bending flexibility	$N^{-1}.m^{-2}$	111.5	106.0
bend/twist coupling	$N^{-1}.m^{-2}$	71.1	58.2

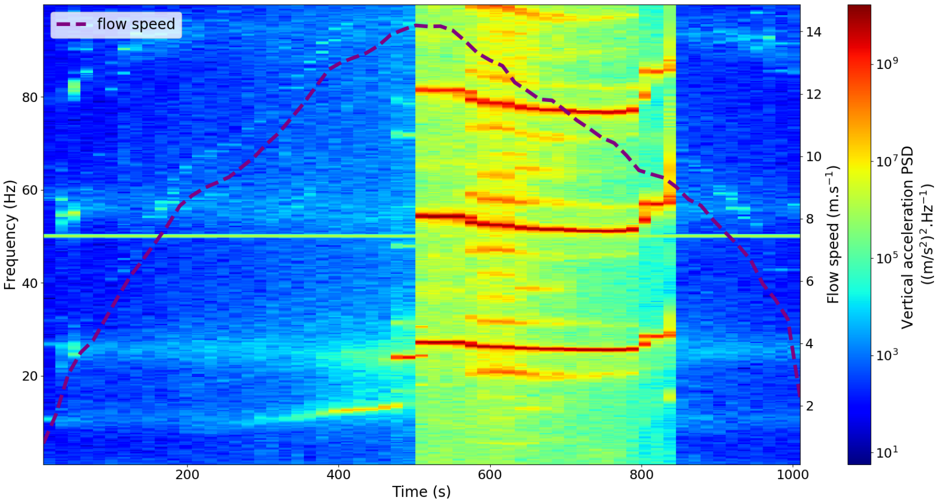

(a)

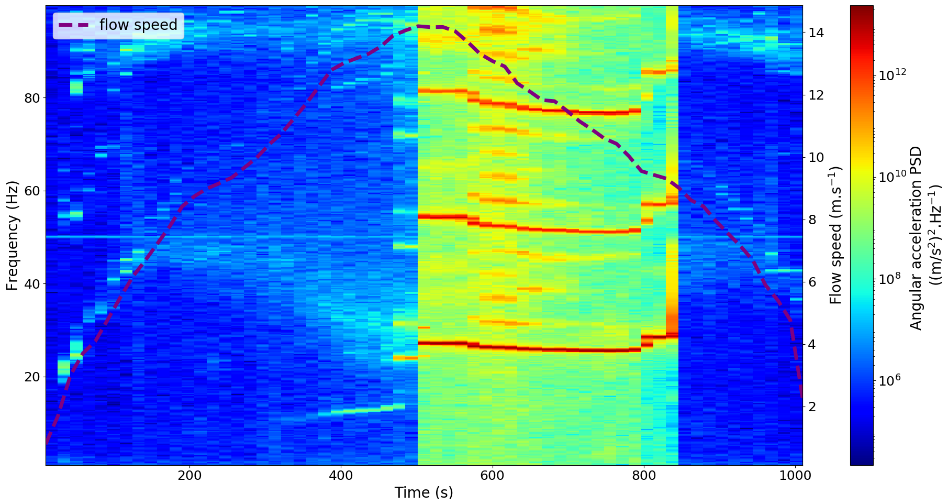

(b)

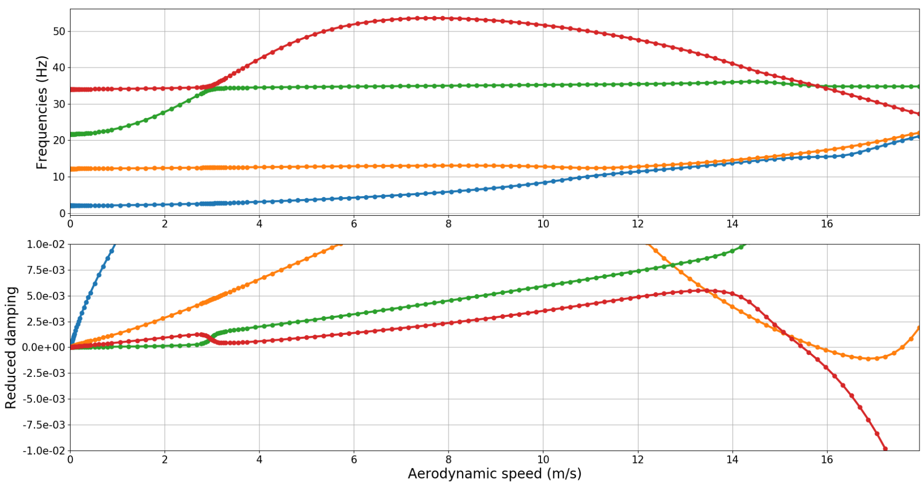

(c)

Figure 7: 420 mm half-span [30, 0, 30] laminate test result: a) vertical acceleration spectrogram, b) angular acceleration spectrogram, c) GEBTAero aeroelastic modes plot.

DOI: 10.13009/EUCASS2019-586

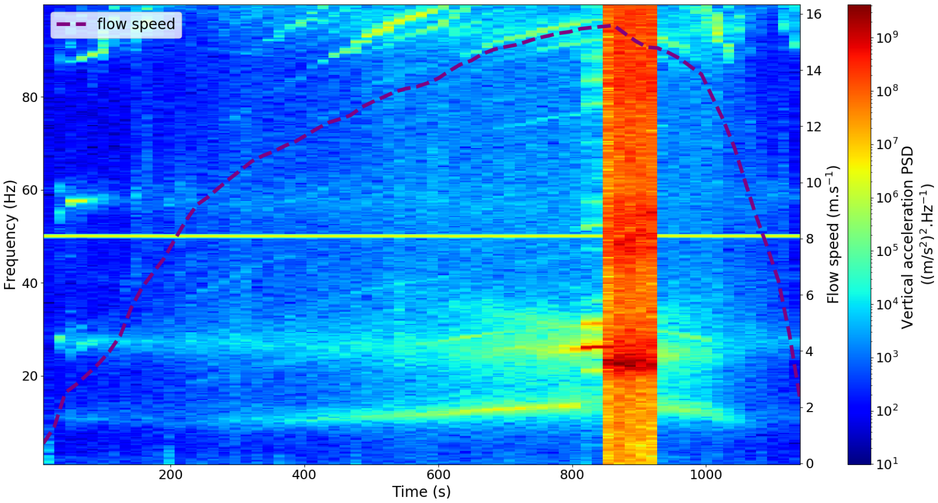

(a)

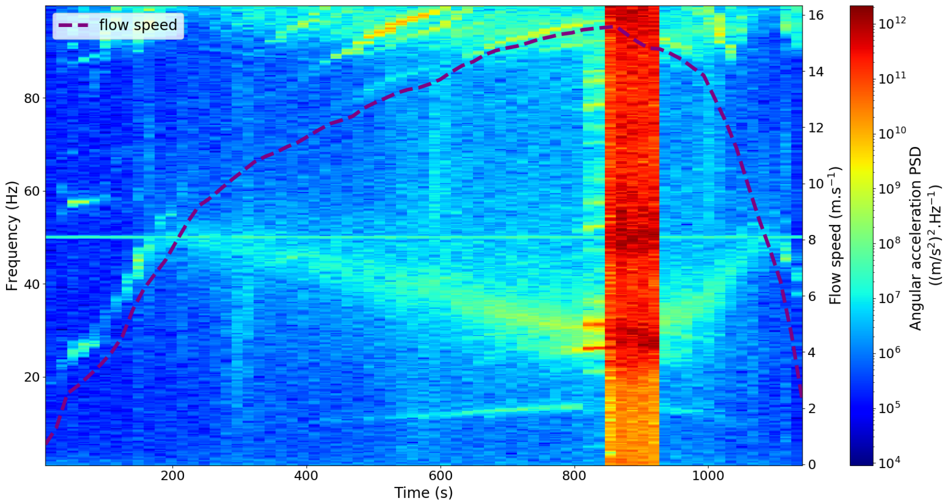

(b)

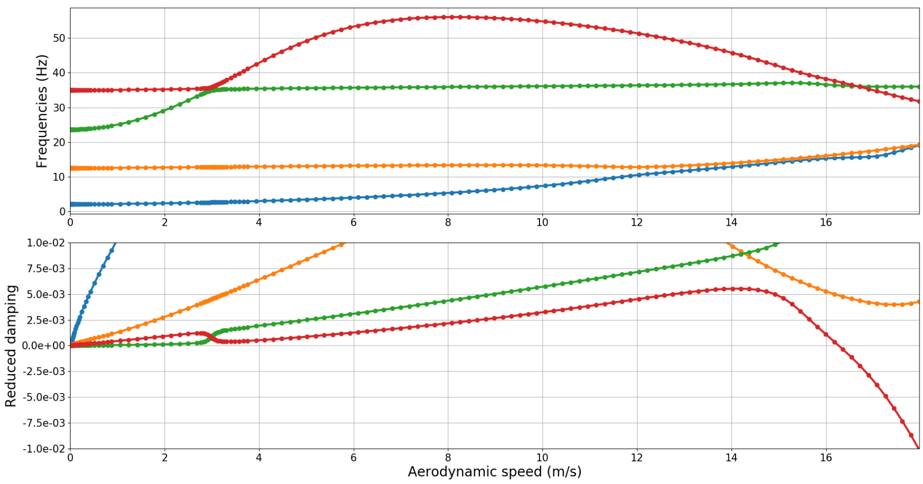

(c)

Figure 8: 420 mm half-span [30, −30, 30] laminate test result: a) vertical acceleration spectrogram, b) angular acceleration spectrogram, c) GEBTAero aeroelastic modes plot.

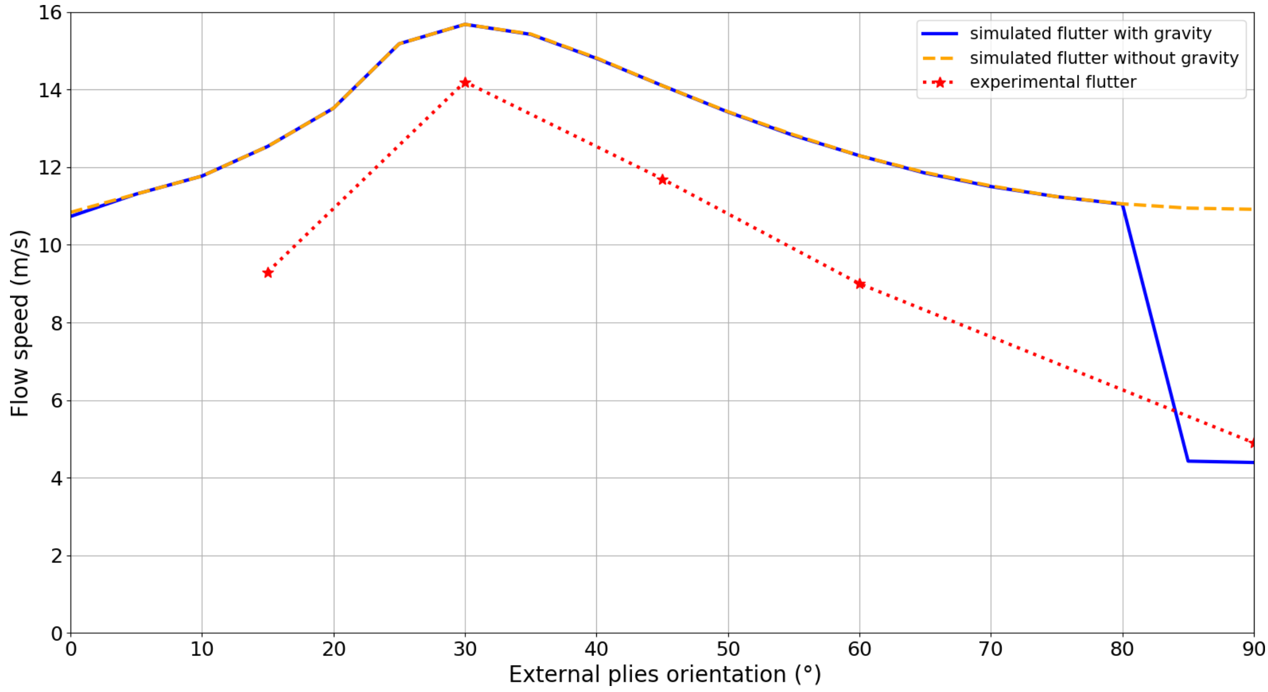

Figure 9: 420 mm half-span $[\theta, 0, \theta]$ laminate flutter speed with a 0° central ply and two variable orientation external plies θ.

the five layups with a central ply oriented at 0°. Regarding frequencies, the first four modes are also plotted. One the one hand, for the flutter speed, the simulation tends to overestimate the value. However, because the vacuum was not perfectly controlled during the cure process, a discrepancy exists in the laminate thickness (measured from 0.48 mm to 0.55 mm instead of the nominal 0.48 mm) while it is a key parameter in terms of aeroelastic behaviour sensitivity, according to CLT. Badly compressed plates tend to be more flexible than expected.

A correction proposed here consist in using the aeroelastic modes visible on angular acceleration PSD, especially in the stable domain, to adjust a unique parameter : the composite ply thickness. To illustrate that, the angular acceleration spectrogram of the layups $[30, 0, 30]$ and $[30, -30, 30]$ are presented (figure 11) with a ply thickness corrected respectively to 0.145 mm and 0.148 mm. The first four aeroelastic modes computed by GEBTAero are superimposed on both spectrogram. Thanks to this unique correction, we can see a good agreement between numerical and experimental aeroelastic modes evolution depending on the flow speed, and a reduction of the flutter speed estimation error.

The other remarkable point on flutter speed (figure 9) is that the bend/twist coupling tends to compensate the effect of the large deflection due to gravity in terms of flutter speed. $[90, 0, 90]$ laminate is the only one impacted by this static deflection. One the other hand, concerning flutter frequency (figure 10), it appears that aeroelastic modes are paired on flutter boundary. Although large errors can be made on simulated flutter frequency, the latter is always close to one the two modes pair. However, the experimental flutter frequency corresponds to a LCO frequency, while simulated flutter frequency corresponds to the one of the unstable mode when the instability starts, as provided by the harmonic analysis.

4. Conclusion

Design challenges induced by HAPS in terms of aeroelastic performances show the need for an accurate reduced order model able to simulate non linear behaviour of an anisotropic high-aspect-ratio wing. The present work presents a solution based of the geometrically exact beam theory coupled with a two-dimensional unsteady finite state aerodynamic model implemented into an open source solver. Accuracy of flutter speed computation on both undeformed and deformed wing has been demonstrated using common aeroelastic test cases. In addition, to emphasise geometrical non linearities and anisotropic capabilities, a wind tunnel campaign is conducted. This paper focuses on the tests conducted on three-ply composite flat plates with external plies oriented in the same direction, which is the simplest layup exhibiting bend/twist coupling usable in a wind tunnel. A particular focus was laid on two layups, $[30, 0, 30]$ and $[30, -30, 30]$, illustrating the complex behaviour of such anisotropic flexible wings, with highly coupled aeroelastic

DOI: 10.13009/EUCASS2019-586

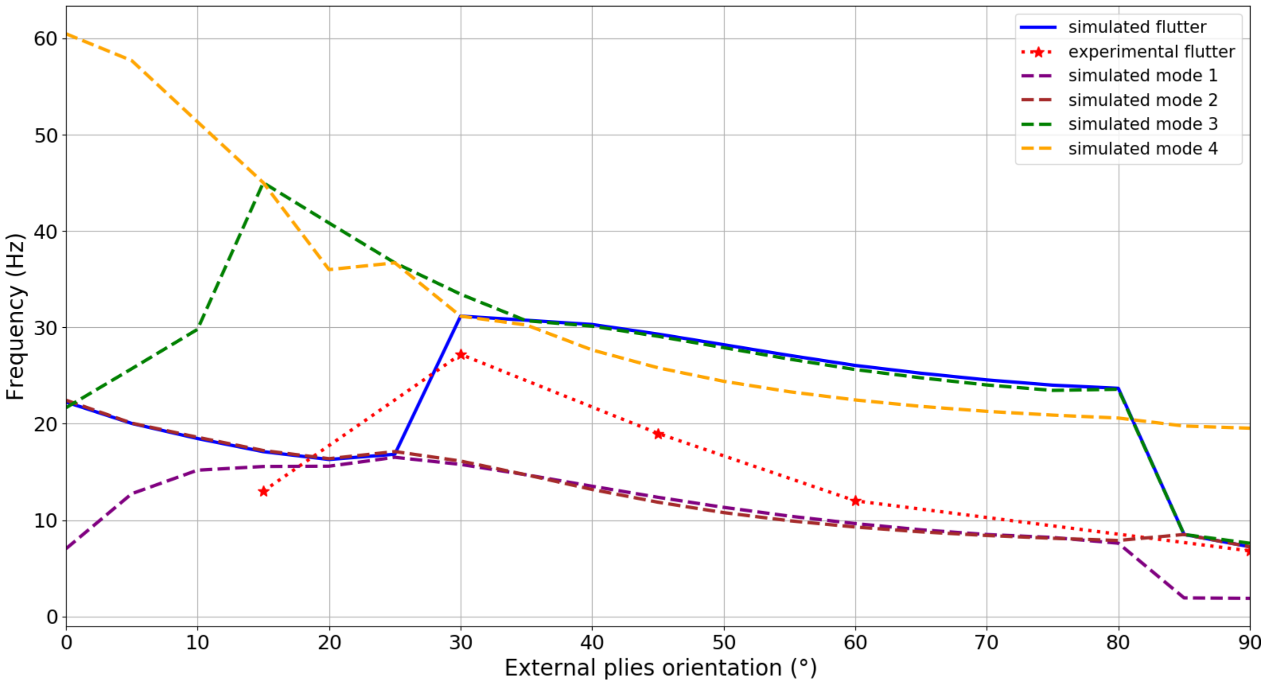

Figure 10: 420 mm half-span $[\theta, 0, \theta]$ laminate first aeroelastic modes and flutter frequencies with a 0° central ply and two variable orientation external plies θ.

modes. Plate thickness appears to be a very sensitive parameters, thus the lamination process is not sufficiently mastered here to allow an adequate comparison between numerical and experimental results. However, a simple, constant spanwise, ply thickness correction allows to produce a promising mode correlation, paving the way for further flexible composite plate experiments.

References

[1] Patrick R. Amestoy, Iain S. Duff, Jean-Yves L'Excellent, and Jacko Koster. A fully asynchronous multifrontal solver using distributed dynamic scheduling. *SIAM Journal on Matrix Analysis and Applications*, 23(1):15–41, 2001.

[2] Patrice Cartraud and Tanguy Messager. Computational homogenization of periodic beam-like structures. *International Journal of Solids and Structures*, 43(3-4):686–696, 2006.

[3] C.-S. Chang, Dewey H. Hodges, and Mayuresh J. Patil. Flight dynamics of highly flexible aircraft. *Journal of Aircraft*, 45(2):538–545, 2008.

[4] G. Dhondt and K. Wittig. Calculix: a free software three-dimensional structural finite Element Program. *MTU Aero Engines GmbH, Munich, Germany*, 1998.

[5] Mark Drela. Integrated simulation model for preliminary aerodynamic, structural, and control-law design of aircraft. *AIAA Paper*, 99:1394, 1999.

[6] Martin Goland. The flutter of a uniform cantilever wing. *Journal of Applied Mechanics-Transactions of the ASME*, 12(4):A197–A208, 1945.

[7] Dewey H. Hodges. A mixed variational formulation based on exact intrinsic equations for dynamics of moving beams. *International journal of solids and structures*, 26(11):1253–1273, 1990.

[8] Dewey H. Hodges and G. Alvin Pierce. *Introduction to structural dynamics and aeroelasticity*, volume 15. Cambridge University Press, 2011.

[9] Bertrand Kirsch. GEBTAero : https://framagit.org/BertrandK/GEBTAero, 2019.

DOI: 10.13009/EUCASS2019-586

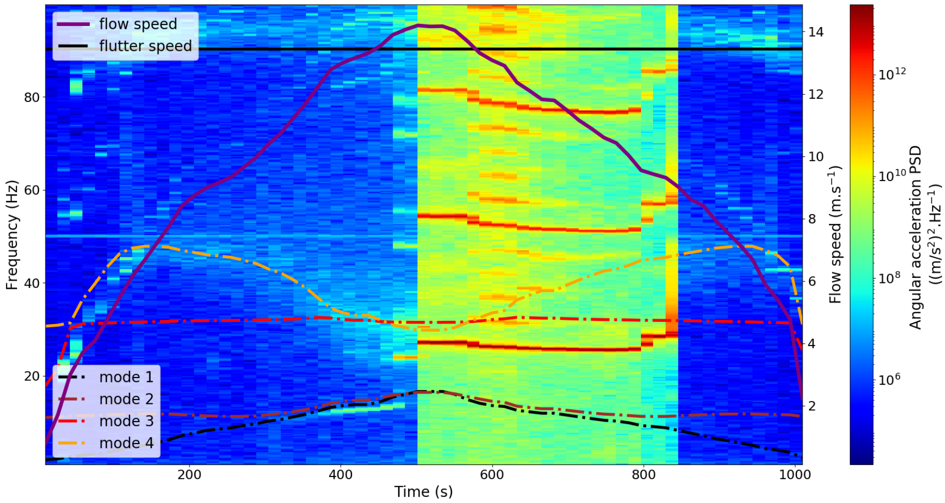

(a)

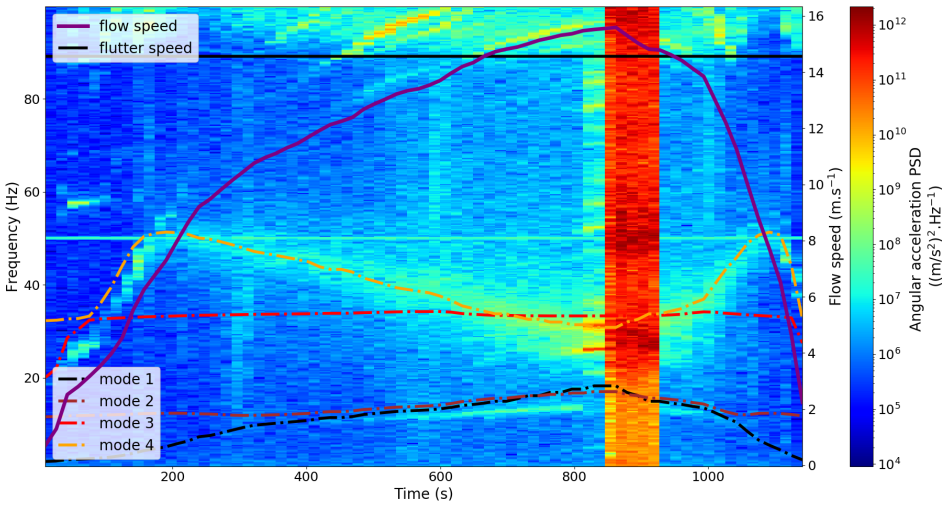

(b)

Figure 11: 420 mm half-span laminate angular acceleration spectrogram with a corrected ply thickness : a) layup $[30, 0, 30]$ with a corrected ply thickness of 0.145 mm, b) layup $[30, -30, 30]$ with a corrected ply thickness of 0.148 mm.

DOI: 10.13009/EUCASS2019-586

[10] Bertrand Kirsch, Olivier Montagnier, Emmanuel Bénard, and Thierry Faure. Assessment of aeroelastic tailoring effect on high-aspect-ratio composite wing flutter speed using an open source reduced order model solver. In *18 th European Conference on Composite Materials*, pages 24 – 28, Athens, Greece, June 2018.

[11] Bertrand Kirsch, Olivier Montagnier, Emmanuel Bénard, and Thierry Faure. Numerical and experimental study of aeroelastic tailoring effect using flexible composite laminates for haps application. In *The International Forum on Aeroelasticity and Structural Dynamics 2019*, Savannah, Georgia, USA, June 2019.

[12] Bertrand Kirsch, Olivier Montagnier, Emmanuel Bénard, and Thierry M. Faure. Open source implementation of a tightly coupled aeroelastic reduced order model suited for aeroelastic tailoring optimisation of high aspect ratio composite wing. *Journal of Fluids and Structures*, under review.

[13] Bertrand Kirsch, Olivier Montagnier, Emmanuel Bénard, and Thierry M. Faure. Computation of very flexible high-aspect-ratio composite wing flutter speed using optimised open source solver. In *53rd 3AF International Conference on Applied Aerodynamics Multiphysics approach in Aerodynamics*, Salon de Provence, France, March 2018.

[14] R. B. Lehoucq, D. C. Sorensen, and C. Yang. ARPACK Users' Guide: Solution of Large Scale Eigenvalue Problems with Implicitly Restarted Arnoldi Methods. *Software Environ. Tools*, 6, 1997.

[15] Eli Livne. Aircraft active flutter suppression: State of the art and technology maturation needs. *Journal of Aircraft*, 55(1):410–452, 2017.

[16] Joseba Murua, Rafael Palacios, and J. Michael R. Graham. Assessment of wake-tail interference effects on the dynamics of flexible aircraft. *AIAA Journal*, 50(7):1575–1585, 2012.

[17] Mayuresh J. Patil. *Nonlinear aeroelastic analysis, flight dynamics, and control of a complete aircraft*. PhD thesis, Citeseer, 1999.

[18] David A. Peters, Swaminathan Karunamoorthy, and Wen-Ming Cao. Finite state induced flow models. I-Two-dimensional thin airfoil. *Journal of Aircraft*, 32(2):313–322, 1995.

[19] Flavio Luiz Cardoso Ribeiro, Pedro Paglione, Roberto Gil Annes da Silva, and Marcelo Santiago de Sousa. Aeroflex: a toolbox for studying the flight dynamics of highly flexible airplanes. In *VII Congresso Nacional de Engenharia Mecânica*, São Luís - Maranhão, Brasil, 2012.

[20] Christopher M. Shearer and Carlos ES Cesnik. Nonlinear flight dynamics of very flexible aircraft. *Journal of Aircraft*, 44(5):1528–1545, 2007.

[21] Deman Tang and Earl Dowell. Experimental aeroelastic models design and wind tunnel testing for correlation with new theory. *Aerospace*, 3(2):12, 2016.

[22] Qi Wang, Wenbin Yu, Michael A. Sprague, and Jason Jonkman. Geometric Nonlinear Analysis of Composite Beams Using Wiener-Milenkovic Parameters. In *Proceedings of the 54th AIAA/ASME/ASCE/AHS/ASC Structures, Structural Dynamics, and Materials Conference and Co-located Events, Boston, Massachusetts*, pages 8–11, 2013.

[23] Zhicun Wang, P. C. Chen, D. D. Liu, and D. T. Mook. Nonlinear-aerodynamics/nonlinear-structure interaction methodology for a high-altitude long-endurance wing. *Journal of Aircraft*, 47(2):556–566, 2010.

[24] Wenbin Yu and Maxwell Blair. GEBT: A general-purpose nonlinear analysis tool for composite beams. *Composite Structures*, 94:2677–2689, September 2012.